

辅助腔增强磁光力系统中的相干光学传输

侯宝成, 陈华俊*

安徽理工大学力学与光电物理学院, 安徽 淮南 232001

摘要 提出了一种双谐振腔模式的磁光力学系统。在该系统中,左右两个光学谐振腔均由能量低的探测场和能量高的泵浦场驱动,其中左侧谐振腔存在机械振动模且与一个磁振子(钇铁石榴石小球)耦合,两个谐振腔的光场之间存在耦合。通过控制该系统中两侧探测场强度的比值、磁振子与腔光子之间的耦合强度、磁振子与机械振子之间的耦合强度以及左右两个谐振腔之间的耦合强度,光力系统会出现模式分裂、完美量子相长相干、完美量子相消相干、磁振子能量的吸收等现象。该系统中左右两个谐振腔之间的耦合起着关键作用,提供了一个量子通道并影响透明窗口的峰值。通过研究和操纵该系统中的参数,实现了对输出场的有效调控。研究结果在量子光学以及光子信息网络构建中有一定的应用前景。

关键词 量子光学; 磁振子; 腔光力系统; 相干光学传输

中图分类号 O431.2

文献标志码 A

DOI: 10.3788/CJL220630

1 引言

近年来,随着激光技术以及纳米技术的飞速发展,光力学器件的空间尺寸不断缩小。作为凝聚态物理以及量子光学的交叉领域,腔光力学在光学器件以及光学实验上的应用得到了众多研究者的关注^[1-5]。许多奇特现象不断被观测到,其中包括光学谐振腔与机械振子之间的强耦合现象^[6-8]、光学模式和机械模式之间的相干转换现象^[9-10]、光力学诱导透明现象等^[11-14]。典型的腔光力学系统结构较为简单,谐振腔的两端有两个平面镜,一个固定而另一个是可以作简谐运动的法布里-珀罗腔^[15]。在光力系统发展的同时,一种由磁振子与谐振腔组成的混合系统即腔磁量子动力学系统受到越来越多的关注,研究者利用该系统主要研究受限或纳米结构系统中自旋波的行为状态,其中磁性系统在腔光力学中的量子特性以及物理应用成为了研究热点,腔磁量子动力学系统已成为实现磁子、腔光子和机械振子三者之间量子相干和耦合的新平台^[16-20]。在腔磁量子动力学的背景下,研究者还研究了磁子暗模^[21]、异常点^[22]、远距离自旋电流的操纵和双稳态^[23]等有趣的现象。其中,腔光子与磁振子的耦合是通过磁偶极子相互作用实现的,而磁致伸缩力是磁振子与声子相互作用的基础。传统的光机械系统主要是利用辐射力^[24-25]、静电力^[26]和压电力^[27]来耦合声子与光子,但它们本质上都缺乏良好的可调谐性,磁致伸缩力的出现

为不同信息载体提供了新的实现途径^[16-17,28]。由于磁振子是磁性的集体激发,其频率可由外加偏置磁场调节,因此选择优良的磁性材料很重要。以钇铁石榴石(YIG)为例,它具有极高的自旋密度和丰富的非线性特性,并在不同的信息载体中具有低损耗的特性,可以实现腔磁量子动力学的超强耦合,这些特性使得其在腔光力学系统和其他量子系统中可能出现更多的有趣和重要的现象,也为实现高可调谐的信息量子系统提供了很好的机会。如磁振子与超导量子位相干耦合^[29]、磁振子与弹性波之间的耦合^[30]、磁振子与声子之间的耦合^[17]等。由于磁振子和腔光子之间有着较低的阻尼率以及强耦合机制,腔磁机械系统的相关领域也在经历着快速的发展。Li等^[16,18]在腔光机械系统中放置一个由磁场直接驱动的YIG小球,在最优参数下实现了磁振子、光子和机械振子之间的三重纠缠。除此之外,研究者还研究了高阶边带的产生^[31]、自旋波克尔效应^[32]、腔磁力学系统的光透射^[33]等。

本文基于Li等^[16,18,34]的研究,设计了一个由谐振腔与磁振子组成的双谐振腔磁力学系统。谐振腔的两侧同时输入控制场和探测场,其中一个微腔存在机械振动,且两个谐振腔的光场之间存在耦合,耦合强度与两谐振腔的间距相关,可以基于辐射压力和电磁场的磁光力效应对该混合系统进行有效调谐。在此基础上通过输入-输出理论分析了双谐振腔磁机械系统。在不同的参数机制下,从腔输出中可以观察到在腔与腔

收稿日期: 2022-03-04; 修回日期: 2022-03-20; 录用日期: 2022-05-25; 网络首发日期: 2022-06-10

基金项目: 国家自然科学基金(11804004, 11647001)、安徽省自然科学基金(1708085QA11)、中国博士后科学基金(2020M681973)、高校优秀青年骨干教师国外访问研修项目(gxgwfx2021024)

通信作者: *chenphysics@126.com

之间的耦合存在的情况下磁振子、光子、声子三者之间的耦合所产生的效应,以及磁振子与光子解耦、磁振子与声子解耦时得到的不同相干特性。这些结果都是电磁诱导透明系统中没有的新现象,可应用到新型的光信息处理器件中^[35-36]。

2 模型与理论

图 1 所示为双谐振腔磁光力系统的模型图,其中谐振腔 a (谐振频率为 ω_a)、机械振子 b (谐振频率为 ω_b) 以及磁振子 m (谐振频率为 ω_m) 三者相互耦合,谐振腔 c 的谐振频率为 ω_c 。谐振腔 a 和谐振腔 c 之间通过能量交换进行耦合,耦合强度 J 随着两谐振腔间距的增加呈指数减小。谐振腔 a 的左侧由一束较强的泵浦激光 ϵ_{s1} (谐振频率为 ω_s , 振幅为 E_{s1}) 和一束较弱的探测激光 ϵ_L (谐振频率为 ω_p , 振幅为 E_L) 驱动,中间放置的是谐

振频率为 ω_m 的 YIG 小球,谐振腔 c 的右侧由一束较强的泵浦激光 ϵ_{s2} (谐振频率为 ω_s , 振幅为 E_{s2}) 和一束较弱的探测激光 ϵ_R (谐振频率为 ω_p , 振幅为 E_R) 驱动。振幅分别定义为 $E_L = \sqrt{\frac{2P_L \kappa}{\hbar \omega_p}}$, $E_R = \sqrt{\frac{2P_R \kappa}{\hbar \omega_p}}$, $E_{s1} = \sqrt{\frac{2P_{s1} \kappa}{\hbar \omega_s}}$, $E_{s2} = \sqrt{\frac{2P_{s2} \kappa}{\hbar \omega_s}}$, 其中 P_L 、 P_R 、 P_{s1} 、 P_{s2} 分别为对应激光的功率, \hbar 为约化普朗克常数, κ 为腔内传输损失引起的光模耗散速率。谐振腔 a 中由激光源直接驱动的磁振子可以与腔光子直接建立耦合机制。将 YIG 小球置于谐振腔 a 的最大磁场中,为了使 YIG 球偏置,需要沿 z 方向施加一个均匀的外偏置磁场;为了使 YIG 球变形,从而达到磁振子动态磁化的目的, y 方向腔模驱动磁场和 z 方向的外偏置磁场同时与 x 方向的腔模磁场垂直。系统的哈密顿量可以表示为

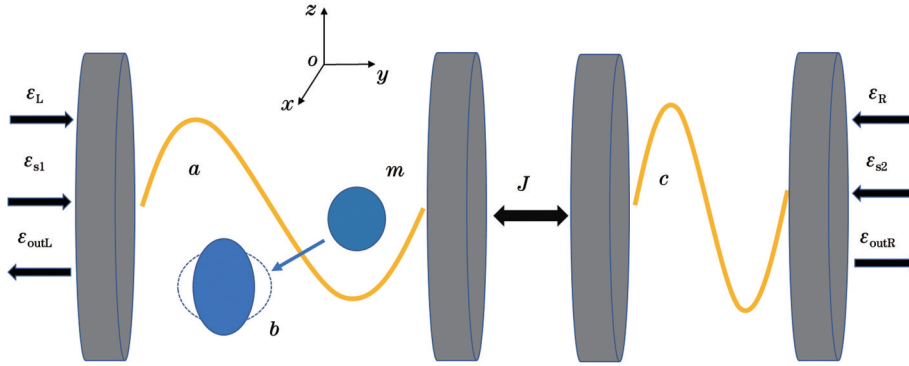


图 1 双微腔磁光力系统

Fig. 1 Dual-microcavity magneto-optomechanical system

$$H = \hbar \Delta_a a^+ a + \hbar \Delta_c c^+ c + \hbar \Delta_m m^+ m + \hbar \omega_b b^+ b + \hbar g_{ma} (a m^+ + a^+ m) + \hbar g_{mb} m^+ m (b^+ + b) + \hbar J (a c^+ + a^+ c) + i \hbar \epsilon_{s1} (a^+ - a) + i \hbar \epsilon_{s2} (c^+ - c) + i \hbar \epsilon_R (c^+ e^{-i\Omega t} - c e^{i\Omega t}) + i \hbar \epsilon_L (a^+ e^{-i\Omega t} - a e^{i\Omega t}), \quad (1)$$

式中: $\Delta_a = \omega_a - \omega_s$ 和 $\Delta_c = \omega_c - \omega_s$ 分别表示左右两个腔模与泵浦场之间的失谐; $\Delta_m = \omega_m - \omega_s$ 表示磁振子与泵浦场之间的失谐; $\Omega = \omega_p - \omega_s$ 表示探测场与泵浦场之间的失谐; t 为时间; $a(a^+)$ 、 $c(c^+)$ 、 $b(b^+)$ 和 $m(m^+)$ 分别表示为左光子、右光子、机械振子和磁振子的玻色子湮灭(产生)算子; g_{ma} 表示磁振子-腔光子的耦合强度; g_{mb} 表示磁振子-声子的耦合强度。分析该系统时可以忽略由辐射压力造成的光子和声子之间的耦合,这主要是因为谐振腔中的波长远大于 YIG 小球的尺寸^[16]。式(1)等号右侧的前两项定义为共振频率为 ω_a (ω_c) 的腔场所对应的哈密顿量,第三项定义为共振频率为 ω_m 的磁振子所对应的哈密顿量,第四项定义为共振频率为 ω_b 的机械模所对应的哈密顿量,第五项和第六项分别定义为系统中腔光子与声子和磁振子耦合产生的相互作用项,第七项定义为两个谐振腔之间的相互作用项,第八项和第九项定义为左侧泵浦场与探测场驱动腔 a 之间的相互作用项,最后两项定义为右侧泵浦场与探测场驱动腔 c 之间的相互作用项。通过

海森堡运动方程对系统进行分析计算,可以得到系统的郎之万方程^[37]为

$$\dot{a} = -(i\Delta_a + \kappa_a) a - i g_{ma} m + \epsilon_{s1} + \epsilon_L e^{-i\Omega t} - i J c + \sqrt{2\kappa} a_{in}, \quad (2)$$

$$\dot{c} = -(i\Delta_c + \kappa_c) c + \epsilon_{s2} + \epsilon_R e^{-i\Omega t} - i J a + \sqrt{2\kappa} c_{in}, \quad (3)$$

$$\dot{m} = -(i\Delta_m + \kappa_m) m - i g_{mb} m (b + b^+) - i g_{ma} a + \sqrt{2\kappa} m_{in}, \quad (4)$$

$$\dot{b} = -(i\omega_b + \gamma_m) b - i g_{mb} m m^+ + \sqrt{\gamma_m} b_{in}, \quad (5)$$

式中: κ_a 是腔 a 的衰减率; κ_c 是腔 c 的衰减率; κ_m 是磁振子 m 的衰减率; γ_m 是力学振子与周围热环境耦合产生的机械阻尼率; a_{in} 、 c_{in} 、 m_{in} 、 b_{in} 分别是左腔光子、右腔光子、力学振子、磁振子在系统中产生的阻尼和噪声项,由于这些噪声项均值都为 0,故可以写成 $\langle a_{in}(t) \rangle = \langle c_{in}(t) \rangle = \langle b_{in}(t) \rangle = \langle m_{in}(t) \rangle = 0$ 。由于系统中探测场的强度远远小于泵浦场的强度 ($\delta O \ll O_s$),可以采用线性化之后的运动方程来描述系统量子力学性质,故将式(2)~(5)中的海森堡算符定义为其平均值与一

个小波动项的和: $O = O_s + \delta O (O = a, b, c, m)$ 。该系统在稳态下的平均值^[4,38]可以表示为

$$a_s = \frac{\epsilon_{s1} (i\Delta + \kappa_m)(i\Delta_c + \kappa_c) - iJ\epsilon_{s2}(i\Delta + \kappa_m)}{(i\Delta_a + \kappa_a)(i\Delta_c + \kappa_c)(i\Delta + \kappa_m) + g_{ma}^2(i\Delta_c + \kappa_c) + J^2(i\Delta + \kappa_m)}, \quad (6)$$

$$c_s = \frac{\epsilon_{s2} - iJ a_s}{i\Delta_c + \kappa_c}, \quad (7)$$

$$b_s = \frac{-ig_{mb}|m_s|^2}{i\omega_b + \gamma_m}, \quad (8)$$

$$m_s = \frac{-ig_{ma} a_s}{i\Delta + \kappa_m}, \quad (9)$$

式中: $\Delta = g_{mb}(b_s^* + b_s) + \Delta_m$ 为磁振子存在时腔场和泵浦场之间的有效失谐, 其中*表示取共轭。可以得到系统涨落项的量子郎之万方程^[37]:

$$\delta\dot{a} = -(i\Delta_a + \kappa_a)\delta a - ig_{ma}\delta m + \epsilon_L e^{-i\Omega t} - iJ\delta c + \sqrt{2\kappa} a_{in}, \quad (10)$$

$$\delta\dot{c} = -(i\Delta_c + \kappa_c)\delta c - iJ\delta a + \epsilon_R e^{-i\Omega t} + \sqrt{2\kappa} c_{in}, \quad (11)$$

$$\delta\dot{m} = -(i\Delta + \kappa_m)\delta m - ig_{mb} m_s (\delta b + \delta b^+) - ig_{ma}\delta a + \sqrt{2\kappa} m_{in}, \quad (12)$$

$$\delta\dot{b} = -(i\omega_b + \gamma_m)\delta b - ig_{mb} (\delta m m_s^* + m_s \delta m^+) + \sqrt{\gamma_m} b_{in\circ} \quad (13)$$

为了更清晰地看到动力学方程的物理性质, 可以引入如下慢变换^[1,35]: $\delta a \rightarrow \delta a e^{-i\Delta_a t}$, $\delta c \rightarrow \delta c e^{-i\Delta_c t}$, $\delta m \rightarrow \delta m e^{-i\Delta t}$, $\delta b \rightarrow \delta b e^{-i\omega_b t}$, $a_{in} \rightarrow a_{in} e^{-i\Delta_a t}$, $c_{in} \rightarrow c_{in} e^{-i\Delta_c t}$, $m_{in} \rightarrow m_{in} e^{-i\Delta t}$, $b_{in} \rightarrow b_{in} e^{-i\omega_b t}$ 。变换后的线性化郎之万方程^[39]为

$$\delta\dot{a} = -\kappa_a \delta a - ig_{ma} \delta m e^{-i\Delta_a t + i\Delta_a t} + \epsilon_L e^{-i(\Omega - \Delta_a)t} - iJ\delta c e^{-i\Delta_c t + i\Delta_c t} + \sqrt{2\kappa} a_{in}, \quad (14)$$

$$\delta\dot{c} = -\kappa_c \delta c - iJ\delta a e^{-i\Delta_a t + i\Delta_a t} + \epsilon_R e^{-i(\Omega - \Delta_c)t} + \sqrt{2\kappa} c_{in}, \quad (15)$$

$$\delta\dot{m} = -\kappa_m \delta m - ig_{mb} m_s (\delta b e^{-i\omega_b t + i\Delta_a t} + \delta b^+ e^{i\omega_b t + i\Delta_a t}) - ig_{ma} \delta a e^{-i\Delta_a t + i\Delta_a t} + \sqrt{2\kappa} m_{in}, \quad (16)$$

$$\delta\dot{b} = -\gamma_m \delta b - ig_{mb} (m_s^* \delta m e^{-i\Delta_a t + i\omega_b t} + m_s \delta m^+ e^{i\Delta_a t + i\omega_b t}) + \sqrt{\gamma_m} b_{in\circ} \quad (17)$$

为了使式(14)~(17)成立, 则该系统由红边带驱动^[3,39] ($\Delta_a \simeq \Delta_c \simeq \Delta_m \simeq \omega_b \simeq \Delta$), 此时可以根据旋转波近似忽略系统的快速振荡项 ($e^{\pm 2i\omega_b t}$)。设系统中热噪声项和阻尼平均值都为 0, 可以得到涨落算符期望值方程^[38]:

$$\langle \delta\dot{a} \rangle = -\kappa_a \delta a - ig_{ma} \delta m + \epsilon_L e^{-i\Omega t} - iJ\delta c, \quad (18)$$

$$\langle \delta\dot{c} \rangle = -\kappa_c \delta c + \epsilon_R e^{-i\Omega t} - iJ\delta a, \quad (19)$$

$$\langle \delta\dot{m} \rangle = -\kappa_m \delta m - ig_{mb} m_s \delta b - ig_{ma} \delta a, \quad (20)$$

$$\langle \delta\dot{b} \rangle = -\gamma_m \delta b - ig_{mb} m_s^* \delta m, \quad (21)$$

式中: $x = \Omega - \omega_b$, 定义为探测场与腔场的有效失谐。将式(18)~(21)中的均值解写成 $\delta O = O_+ e^{-i\Omega t} + O_- e^{i\Omega t}$ (其中 $O = a, m, b, c$) 形式, 用相关的代换求解方程, 可以得到下列结果^[3,37]

$$a_+ = \frac{(\kappa_c - i\Omega) \epsilon_L - iJ \epsilon_R}{Ag_{ma}^2 (\gamma_m - i\Omega)(\kappa_c - i\Omega) + (\kappa_a - i\Omega)(\kappa_c - i\Omega) + J^2}, \quad (22)$$

$$c_+ = \frac{\epsilon_R - iJ\delta a_+}{\kappa_c - i\Omega}, \quad (23)$$

$$b_+ = \frac{-ig_{mb} m_s^* m_+}{\gamma_m - i\Omega} = -\frac{iG m_+}{\gamma_m - i\Omega}, \quad (24)$$

$$m_+ = -ig_{ma} A (\gamma_m - i\Omega) a_+, \quad (25)$$

式中: $G = g_{mb}|m_s|$ 定义为有效光机械耦合率; $A = \frac{1}{(\kappa_m - i\Omega)(\gamma_m - i\Omega) + G^2}$ 。由光腔的输入-输出关系, 可以确立左右两个谐振腔场与输出场之间的关系表达式^[37,39]为

$$\epsilon_{outL} + \epsilon_L e^{-i\Omega t} = 2\kappa_a \langle a \rangle, \epsilon_{outR} + \epsilon_R e^{-i\Omega t} = 2\kappa_c \langle c \rangle. \quad (26)$$

与式(26)类似, 可以将腔场输出表达式^[40]定义为

$$\epsilon_{outL} = \epsilon_{outL+} e^{-i\Omega t} + \epsilon_{outL-} e^{i\Omega t}, \epsilon_{outR} = \epsilon_{outR+} e^{-i\Omega t} + \epsilon_{outR-} e^{i\Omega t}. \quad (27)$$

因为探测场的输出分量 $\epsilon_{outL+} + (\epsilon_{outR+})$ 与探测场 $\epsilon_L + (\epsilon_R)$ 具有相同的斯托克斯频率 ω_p , 且腔光机械系统的光力相互作用是非线性混频过程, $\epsilon_{outL-} - (\epsilon_{outR-})$ 具有相同的反斯托克斯频率 $2\omega_s - \omega_p$ 。根据式(22)~(27), 可以得到本文所需要的输出分量^[3]为

$$\epsilon_{outL+} = 2\kappa_a a_+ - \epsilon_L, \epsilon_{outR+} = 2\kappa_c c_+ - \epsilon_R. \quad (28)$$

为了研究光响应的光学传输特性, 可以对系统的透射系数和反射系数进行如下描述^[38-40]:

$$T_L = |\epsilon_{outR+} / \epsilon_L|^2, R_L = |\epsilon_{outL+} / \epsilon_L|^2. \quad (29)$$

3 数值结果与讨论

为探究该双谐振腔磁光力机械系统的光响应传输特性, 本文采用实验可行的参数^[14,16]: $\kappa = \kappa_a / (2\pi) = \kappa_c / (2\pi) = 1 \text{ MHz}$, $\gamma_m / (2\pi) = 100 \text{ Hz}$, $\omega_b / (2\pi) = 10 \text{ MHz}$, $g_{ma} = 4 \times \kappa_a$, $\omega_a / (2\pi) = \omega_c / (2\pi) = 10 \text{ GHz}$ 。设定驱动谐振腔 a 的探测光与驱动谐振腔 c 的探测光强度比值为 $n = \epsilon_R / \epsilon_L$ 。主要探讨了两个谐振腔之间的耦合强度 J 、腔 a 与腔 c 的探测光强度比值 n 以及磁振子与系统耦合或解耦对观测系统的影响。通过研究以上几种不同参数机制在系统相互作用情况下的相干光响应, 观测了光力系统的光响应传输特性。

3.1 机械振子与磁振子耦合

图 2 讨论的是系统中磁振子与光子解耦 ($g_{ma} = 0$) 对系统光响应传输特性的影响。比较图 2(a)、(b) 可以看到, 当关闭右侧探测光 ($n = 0$) 时, 即 $\epsilon_L \neq 0, \epsilon_R =$

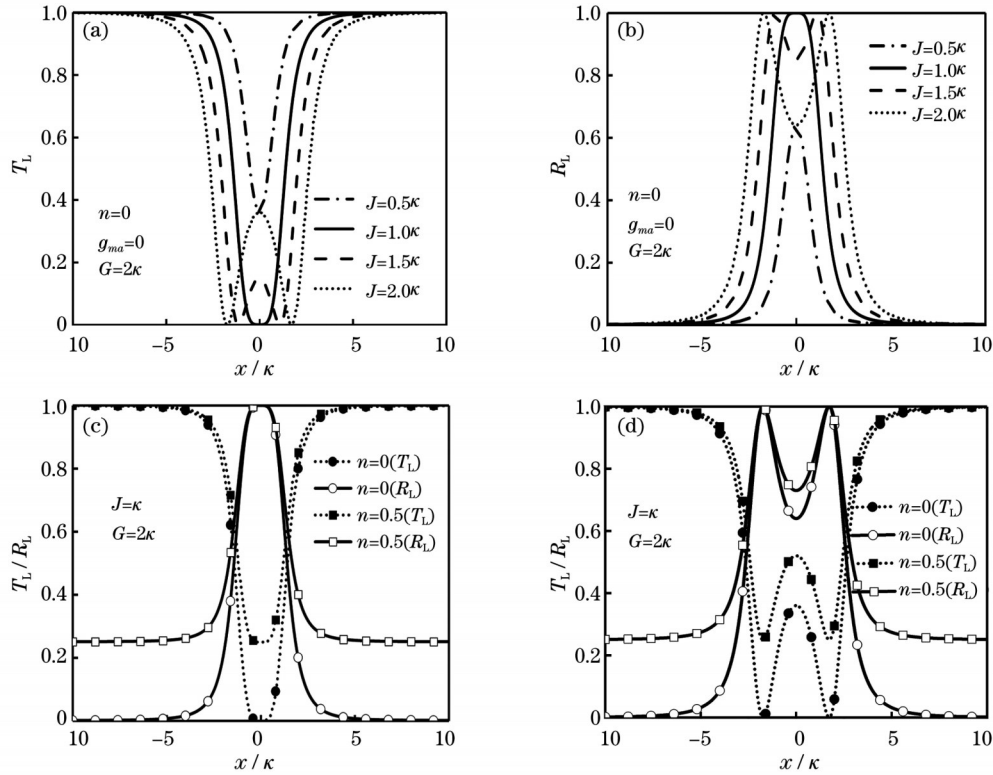


图 2 不同条件下 T_L 和 R_L 随 x/κ 的变化。(a)(b) 不同 J ; (c)(d) 不同 n
 Fig.2 T_L and R_L versus x/κ under different conditions. (a)(b) Different J ; (c)(d) different n

0, 在 $|\epsilon_{outL+}/\epsilon_L| = 0, |\epsilon_{outR+}/\epsilon_L| = 1$ 的条件下, 可以解得 $x = \pm\sqrt{J^2 - \kappa^2}$ 。当耦合强度 $J < \kappa$ 时, $x = \pm\sqrt{J^2 - \kappa^2}$ 没有实数解, 耦合强度 J 越大, 系统透射程度越明显; 当耦合强度 J 的值增大到 $J = \kappa$ 时, 刚好在 J 处有一个实根, 光力系统在中央共振处出现完全透射现象; 当 $J > \kappa$ 时, 系统会出现模式分裂现象, $x = \pm\sqrt{J^2 - \kappa^2}$ 有两个互为相反数的非零实根。因此, 我们可以通过调节两个谐振腔耦合强度 J 所对应的参数来调节发生透射时的频率, 此时系统可以应用于光开关、光学调制器量子信息处理方面。在图 2(c)、(d) 中, 可以看到, 当两谐振腔之间的耦合强度一定时, 随着谐振腔 c 右侧探测光逐渐增强, 光力系统的透射峰强度逐渐减弱; 当右侧探测光强度相同时, 两谐振腔耦合强度 J 的变化只会改变透明峰的位置, 透射峰的强度并没有发生变化。这是因为腔与腔之间的耦合强度不会对机械振子与磁振子之间的耦合造成破坏性的影响。

3.2 光子与磁振子耦合

图 3 讨论的是系统中机械振子与磁振子解耦 ($g_{mb} = 0$) 对系统光响应传输特性的影响。从图 3(a)~(c) 可以看到, 当关闭谐振腔右侧探测光 ($n = 0$) 并固定光子与磁振子之间的耦合强度 (g_{ma}) 时, 在两个谐振腔之间的耦合强度 J 较弱的条件下, 光力系统的透射率与反射率并不明显, 随着两个谐振腔之间的耦合强度 J 的增加, 两侧透明峰的峰值逐渐增大, 而中央共振处的强度逐渐减小。从图 3(d)、(e) 可以看到, 当左右

探测光的强度相同 ($n = 1$) 时, 随着 J 的增大, 左侧腔的透射率和反射率峰值明显增大。这是因为当两谐振腔之间的耦合强度 $J = 2\kappa$ 时, 双谐振腔磁机械系统的一侧探测场出现全透射, 而谐振腔另一侧同时出现全反射, 左右两个探测场发生完美量子相干, 也就是在一侧出现完美量子相长相干, 而另一侧同时出现完美量子相消相干。在固定光子与磁振子之间的耦合强度 (g_{ma}) 时, 随着两个谐振腔之间的耦合强度 J 的增加, 两侧透明峰的峰值逐渐增大, 但透明峰的间距不发生变化。

从图 3(e)、(f) 可以看到, 当左右探测光的强度相同 ($n = 1$) 且固定两个谐振腔之间的耦合强度 J 时, 随着光子与磁振子之间的耦合强度 (g_{ma}) 的增加, 两侧透明峰明显向外平移, 导致透明峰的间距变大, 所以可以通过控制耦合强度 g_{ma} 来调控两透明峰的有效距离。同时, 可以看到, 随着 g_{ma} 的增大, 两侧透明峰的峰值减小。这是由于在增大光子与磁振子之间耦合强度时, 其中一部分能量会储存到磁振子中。

3.3 光子、机械振子与磁振子的三重耦合

图 4、5 讨论的是系统中光子、机械振子与磁振子的三者耦合对系统光响应传输特性的影响。从图 4(a)~(c) 可以看到, 当关闭谐振腔 c 右侧探测光 ($n = 0$) 且增强两个谐振腔之间的耦合强度 J 时, 两侧透明峰的峰值逐渐变大, 中央共振处的峰值逐渐变小, 并且在 $J = 2\kappa$ 时出现标准的模式分裂现象 [图 4(c)]。当改变有效光机械耦合率时, 随着 G 值的增大, 中央共振处的透明峰宽度变大, 两侧透明峰的间距增大,

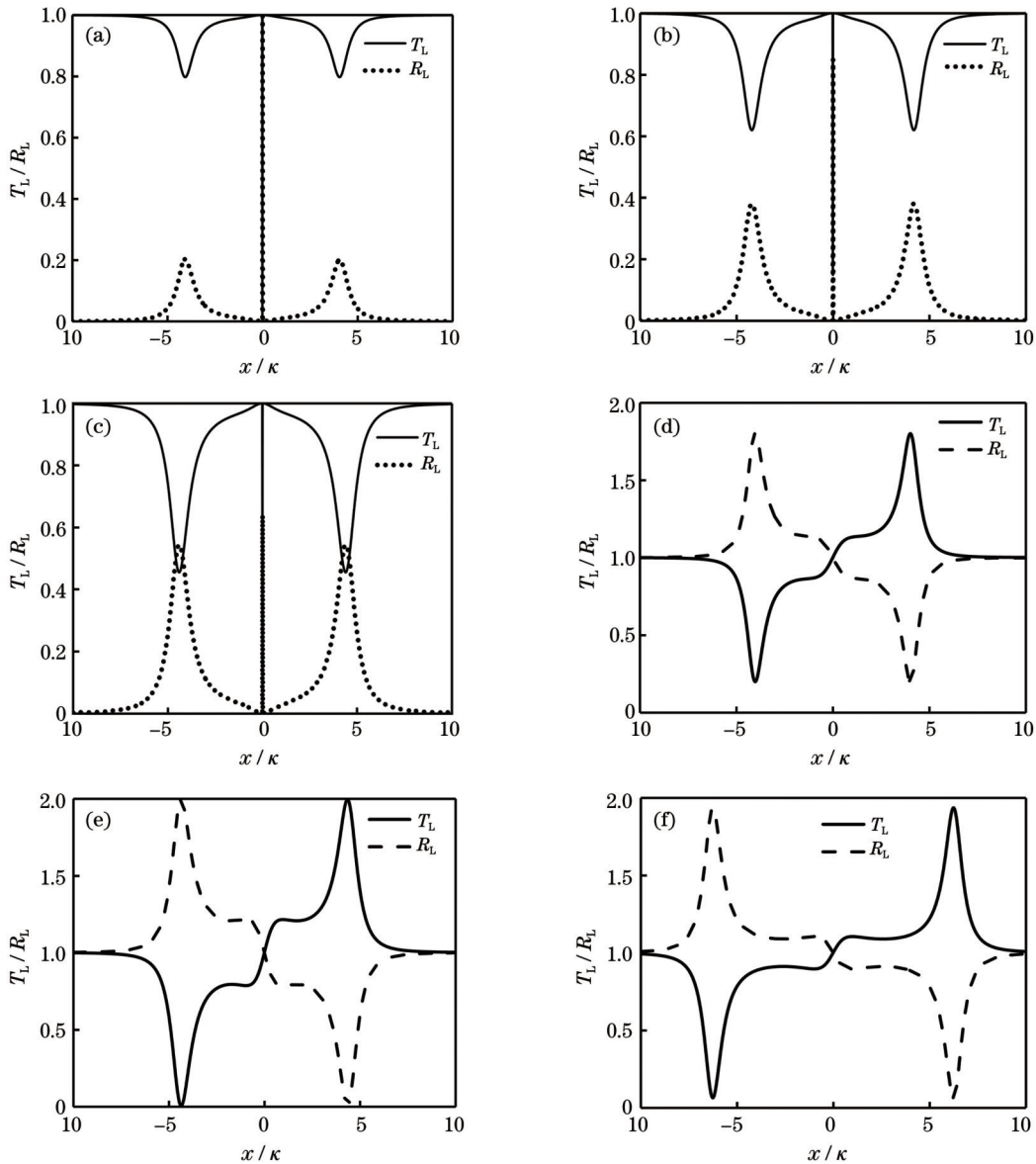


图 3 不同条件下 T_L 和 R_L 随 x/κ 的变化。(a) $n=0, J=\kappa, g_{ma}=4\kappa$; (b) $n=0, J=1.5\kappa, g_{ma}=4\kappa$; (c) $n=0, J=2\kappa, g_{ma}=4\kappa$;
(d) $n=1, J=\kappa, g_{ma}=4\kappa$; (e) $n=1, J=2\kappa, g_{ma}=4\kappa$; (f) $n=1, J=2\kappa, g_{ma}=6\kappa$

Fig.3 T_L and R_L versus x/κ under different conditions. (a) $n=0, J=\kappa, g_{ma}=4\kappa$; (b) $n=0, J=1.5\kappa, g_{ma}=4\kappa$; (c) $n=0, J=2\kappa, g_{ma}=4\kappa$;
(d) $n=1, J=\kappa, g_{ma}=4\kappa$; (e) $n=1, J=2\kappa, g_{ma}=4\kappa$; (f) $n=1, J=2\kappa, g_{ma}=6\kappa$

但两侧透明峰的峰值减小,这是由于机械振子与磁振子之间的耦合也会使一部分能量储存到磁振子中。如图 3(a)~(c)所示,光力系统中声子与磁振子的解耦($G=0$)导致中央共振处透明峰的宽度趋近于0。

图 5 讨论的是当系统左右探测光的强度相同($n=1$)时光子、机械振子与磁振子的三重耦合对系统透射率和反射率的影响。由于系统两侧探测场量子相干的影响,在系统同时存在光子、机械振子与磁振子的三重耦合时,光力系统两侧均会出现透射率先增大后减小而反射率先减小后增大的现象。这种现象非常重要,基于这个现象对弱光信号的动力学传播过程进行动态调控,可以构造一些特殊功能的光子学器件,如光子路由器、光子转换器等。在这些光子学器件中,光子不

仅是构成信息流的单位,还具备控制设备的功能,这些器件在量子计算机的构建中有一定的应用前景。随着两个谐振腔之间的耦合强度 J 的增加,两侧透明峰以及中央共振处的峰值会逐渐增大,但透明峰的间距不会改变,如图 5(a)、(b)所示。随着光子与磁振子之间的耦合强度(g_{ma})的增加,两侧透明峰的间距增加,中央透明峰的峰值变大,同时两侧透明峰的峰值减小。这是因为光子与磁振子之间的耦合导致系统储存到磁振子中的能量主要由两侧透明峰提供,如图 5(c)所示。随着有效光机械耦合强度的增加,两侧透明峰的间距增加,峰值变大,同时中央透明峰的峰值减小。这是因为机械振子与磁振子之间的耦合导致系统储存到磁振子中的能量主要由中央透明峰提供,如图 5(d)所示。

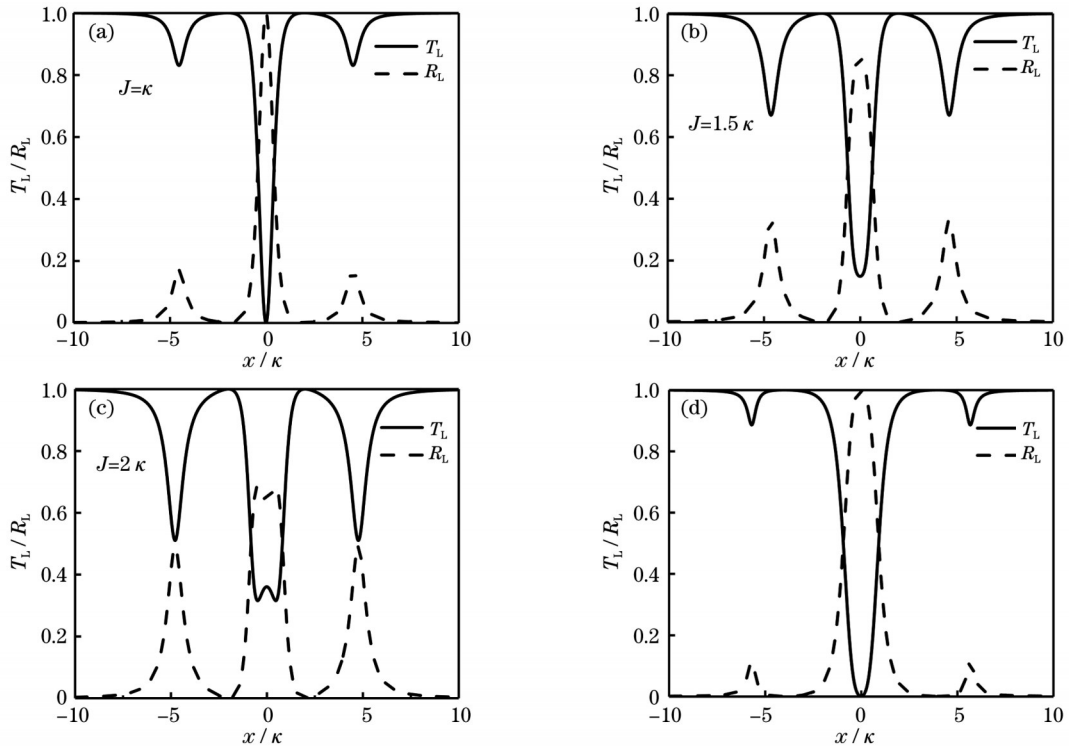


图 4 不同条件下 T_L 和 R_L 随 x/κ 的变化。(a)~(c) $n=0, g_{ma}=4\kappa, G=2\kappa$, 不同 J ; (d) $n=0, J=\kappa, g_{ma}=4\kappa, G=4\kappa$

Fig.4 T_L and R_L versus x/κ under different conditions. (a)~(c) $n=0, g_{ma}=4\kappa, G=2\kappa$, and different J ; (d) $n=0, J=\kappa, g_{ma}=4\kappa, G=4\kappa$

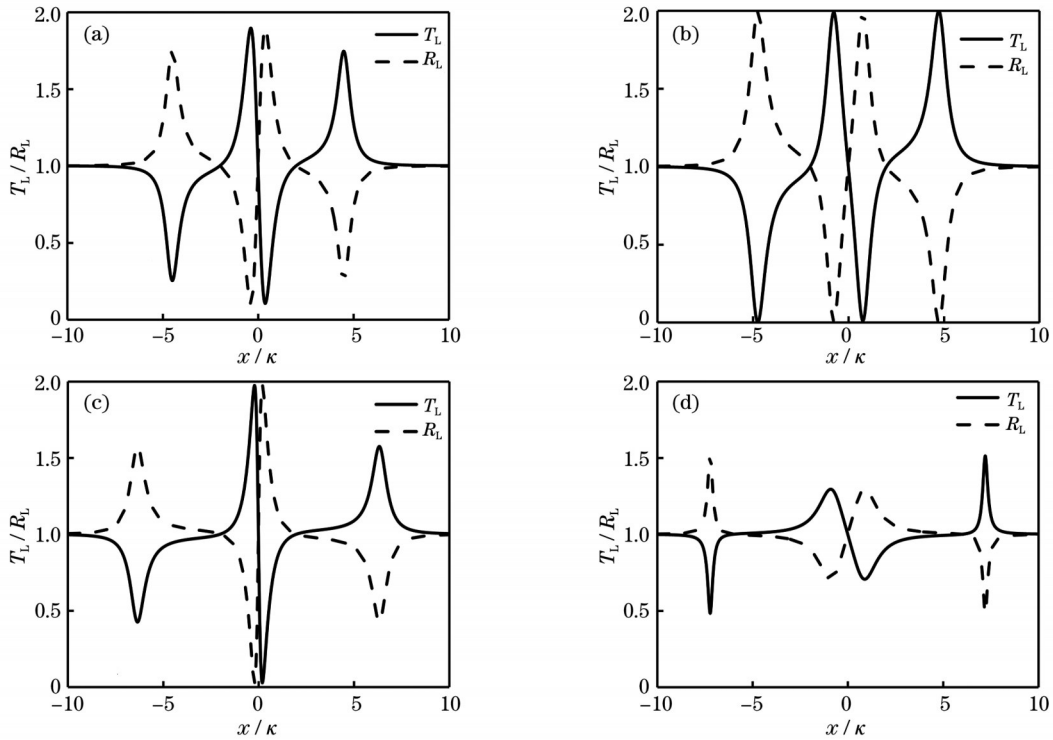


图 5 不同条件下 T_L 和 R_L 随 x/κ 的变化。(a) $n=1, J=\kappa, g_{ma}=4\kappa, G=2\kappa$; (b) $n=1, J=2\kappa, g_{ma}=4\kappa, G=2\kappa$; (c) $n=1, J=\kappa, g_{ma}=6\kappa, G=2\kappa$; (d) $n=1, J=\kappa, g_{ma}=6\kappa, G=6\kappa$

Fig.5 T_L and R_L versus x/κ under different conditions. (a) $n=1, J=\kappa, g_{ma}=4\kappa, G=2\kappa$; (b) $n=1, J=2\kappa, g_{ma}=4\kappa, G=2\kappa$; (c) $n=1, J=\kappa, g_{ma}=6\kappa, G=2\kappa$; (d) $n=1, J=\kappa, g_{ma}=6\kappa, G=6\kappa$

4 结 论

在光机械系统的基础上,提出了一种基于磁振子

的双谐振腔磁光力机械系统。在该系统两侧同时输入强泵浦场和弱探测场,调节腔与腔之间的耦合强度和两侧的探测光强度比值等参数。结果显示,在磁振子

与机械振子耦合、磁振子与光子耦合、三者共同耦合这些不同的机制下,通过调节系统参数来调控探测场,该双谐振腔磁机械系统会出现完全不同的光学传输特性,如模式分裂、完美量子相长相干、完美量子相消相干、磁振子能量吸收等,这在量子信息处理过程中是非常重要的。研究结果有利于从新的角度理解腔光力系统相关的现象,为可控光子传输和新型光子器件的研究提供了参考。

参 考 文 献

- [1] Agarwal G S, Huang S M. Nanomechanical inverse electromagnetically induced transparency and confinement of light in normal modes[J]. *New Journal of Physics*, 2014, 16(3): 033023.
- [2] 侯宝成, 陈华俊. 基于磁光力系统的相干光学传输特性研究[J]. *光学学报*, 2021, 41(21): 2127001.
Hou B C, Chen H J. Coherent optical transmission characteristics based on magneto-optical force system[J]. *Acta Optica Sinica*, 2021, 41(21): 2127001.
- [3] Chen H J. Multiple-Fano-resonance-induced fast and slow light in the hybrid nanomechanical-resonator system[J]. *Physical Review A*, 2021, 104(1): 013708.
- [4] 喻富, 肖添, 何高倩, 等. 超导量子比特耦合微波腔和机械谐振器系统的探测场吸收特性研究[J]. *激光与光电子学进展*, 2022, 59(3): 0327001.
Yu F, Xiao T, He G Q, et al. Probe absorption properties of a superconducting qubit coupled to microwave cavity and mechanical resonator[J]. *Laser & Optoelectronics Progress*, 2022, 59(3): 0327001.
- [5] 张天才, 毋伟, 杨鹏飞, 等. 高精度度法布里-珀罗光学微腔及其在强耦合腔量子电动力学中的应用[J]. *光学学报*, 2021, 41(1): 0127001.
Zhang T C, Wu W, Yang P F, et al. High-finesse micro-optical Fabry-Perot cavity and its applications in strongly coupled cavity quantum electrodynamics[J]. *Acta Optica Sinica*, 2021, 41(1): 0127001.
- [6] Balram K C, Davanço M I, Song J D, et al. Coherent coupling between radiofrequency, optical and acoustic waves in piezo-optomechanical circuits[J]. *Nature Photonics*, 2016, 10(5): 346-352.
- [7] Aspelmeyer M, Kippenberg T J, Marquardt F. Cavity optomechanics[J]. *Reviews of Modern Physics*, 2014, 86(4): 1391-1452.
- [8] 李刚, 张鹏飞, 杨鹏飞, 等. 光学腔与原子强耦合的实验研究进展[J]. *光学学报*, 2022, 42(3): 0327005.
Li G, Zhang P F, Yang P F, et al. Experimental progress of strongly coupling between optical cavity and atoms[J]. *Acta Optica Sinica*, 2022, 42(3): 0327005.
- [9] Fiore V, Yang Y, Kuzyk M C, et al. Storing optical information as a mechanical excitation in a silica optomechanical resonator[J]. *Physical Review Letters*, 2011, 107(13): 133601.
- [10] Zhou X, Hocke F, Schliesser A, et al. Slowing, advancing and switching of microwave signals using circuit nanoelectromechanics [J]. *Nature Physics*, 2013, 9(3): 179-184.
- [11] Safavi-Naeini A H, Alegre T P M, Chan J, et al. Electromagnetically induced transparency and slow light with optomechanics[J]. *Nature*, 2011, 472(7341): 69-73.
- [12] Weis S, Rivière R, Deléglise S, et al. Optomechanically induced transparency[J]. *Science*, 2010, 330(6010): 1520-1523.
- [13] Agarwal G S, Huang S M. Electromagnetically induced transparency in mechanical effects of light[J]. *Physical Review A*, 2010, 81(4): 041803.
- [14] Chen H J. High-resolution biomolecules mass sensing based on a spinning optomechanical system with phonon pump[J]. *Applied Physics Express*, 2021, 14(8): 082005.
- [15] Kleckner D, Bouwmeester D. Sub-kelvin optical cooling of a micromechanical resonator[J]. *Nature*, 2006, 444(7115): 75-78.
- [16] Li J, Zhu S Y, Agarwal G S. Magnon-photon-phonon entanglement in cavity magnomechanics[J]. *Physical Review Letters*, 2018, 121(20): 203601.
- [17] Zhang X F, Zou C L, Jiang L, et al. Cavity magnomechanics[J]. *Science Advances*, 2016, 2(3): e1501286.
- [18] Li J, Zhu S Y, Agarwal G S. Squeezed states of magnons and phonons in cavity magnomechanics[J]. *Physical Review A*, 2019, 99(2): 021801.
- [19] Liu Z X, Wang B, Kong C, et al. Magnetic-field-dependent slow light in strontium atom-cavity system[J]. *Applied Physics Letters*, 2018, 112(11): 111109.
- [20] Zhang G Q, You J Q. Higher-order exceptional point in a cavity magnonics system[J]. *Physical Review B*, 2019, 99(5): 054404.
- [21] Zhang X F, Zou C L, Zhu N, et al. Magnon dark modes and gradient memory[J]. *Nature Communications*, 2015, 6: 8914.
- [22] Zhang D K, Luo X Q, Wang Y P, et al. Observation of the exceptional point in cavity magnon-polaritons[J]. *Nature Communications*, 2017, 8: 1368.
- [23] Wang Y P, Zhang G Q, Zhang D K, et al. Bistability of cavity magnon polaritons[J]. *Physical Review Letters*, 2018, 120(5): 057202.
- [24] Chen H J. Controllable fast and slow light in the hybrid quantum dot-nanomechanical resonator system mediated by another nanomechanical resonator with Coulomb interaction[J]. *Journal of Applied Physics*, 2021, 130(20): 204302.
- [25] Li W L, Li C, Song H S. Quantum synchronization in an optomechanical system based on Lyapunov control[J]. *Physical Review E*, 2016, 93(6): 062221.
- [26] Andrews R W, Peterson R W, Purdy T P, et al. Bidirectional and efficient conversion between microwave and optical light[J]. *Nature Physics*, 2014, 10(4): 321-326.
- [27] Fan L R, Fong K Y, Poot M, et al. Cascaded optical transparency in multimode-cavity optomechanical systems[J]. *Nature Communications*, 2015, 6: 5850.
- [28] Kittel C. Interaction of spin waves and ultrasonic waves in ferromagnetic crystals[J]. *Physical Review*, 1958, 110(4): 836-841.
- [29] Tabuchi Y, Ishino S, Noguchi A, et al. Coherent coupling between a ferromagnetic magnon and a superconducting qubit[J]. *Science*, 2015, 349(6246): 405-408.
- [30] Sinha K P, Upadhyaya U N. Phonon-magnon interaction in magnetic crystals[J]. *Physical Review*, 1962, 127(2): 432-439.
- [31] Liu Z X, Wang B, Xiong H, et al. Magnon-induced high-order sideband generation[J]. *Optics Letters*, 2018, 43(15): 3698-3701.
- [32] Wang Y P, Zhang G Q, Zhang D K, et al. Magnon Kerr effect in a strongly coupled cavity-magnon system[J]. *Physical Review B*, 2016, 94(22): 224410.
- [33] Wang B, Liu Z X, Kong C, et al. Magnon-induced transparency and amplification in PT-symmetric cavity-magnon system[J]. *Optics Express*, 2018, 26(16): 20248-20257.
- [34] Kong C, Xiong H, Wu Y. Magnon-induced nonreciprocity based on the magnon Kerr effect[J]. *Physical Review Applied*, 2019, 12(3): 034001.
- [35] Qin F, Liu Y, Meng Z M, et al. Design of Kerr-effect sensitive microcavity in nonlinear photonic crystal slabs for all-optical switching[J]. *Journal of Applied Physics*, 2010, 108(5): 053108.
- [36] Yang S, Al-Amri M, Evers J, et al. Controllable optical switch using a Bose-Einstein condensate in an optical cavity[J]. *Physical Review A*, 2011, 83(5): 053821.
- [37] Yan X B, Cui C L, Gu K H, et al. Coherent perfect absorption, transmission, and synthesis in a double-cavity optomechanical system[J]. *Optics Express*, 2014, 22(5): 4886-4895.
- [38] Du L, Liu Y M, Zhang Y, et al. All-optical photon transmission switching in a passive-active optomechanical system[EB/OL].

(2018-01-08)[2021-05-06]. <https://arxiv.org/abs/1801.02296>.

- [39] Chen H J, Hou B C, Yang J Y. Controllable coherent optical response in a ring cavity optomechanical system[J]. *Physica E: Low-Dimensional Systems and Nanostructures*, 2021, 125:

114394.

- [40] Du L, Liu Y M, Jiang B, et al. All-optical photon switching, router and amplifier using a passive-active optomechanical system [J]. *EPL (Europhysics Letters)*, 2018, 122(2): 24001.

Coherent Optical Transmission in Magneto-Optomechanical Systems Enhanced by Auxiliary Cavity

Hou Baocheng, Chen Huajun*

School of Mechanics and Optoelectronic Physics, Anhui University of Science and Technology, Huainan 232001, Anhui, China

Abstract

Objective As an interdisciplinary subject of nanophysics and quantum optics, the physical properties of cavity optomechanics have attracted the attention of many researchers. At the same time, with the development of optomechanical systems, cavity magnetic quantum dynamics systems have become a new platform for realizing quantum coherence and coupling between magnons, cavity photons, and mechanical oscillators. This paper proposes the simultaneous input of the control field and detection on both sides. The cavity field (one of the microcavities has a mechanical vibration mode, there is mutual coupling between the optical fields of the two resonators, and the coupling strength is related to the distance between the two resonators) and the dual-resonator magnetomechanical system are composed of magnons. On this basis, the input-output theory is used to analyze the dual-resonator magnetomechanical system under different parameter mechanisms. In the cavity output, magnons, microwave photons, and acoustics can be observed in the presence of cavity-to-cavity coupling. Various coherent properties arise from the coupling between magnons, cavity photons, and mechanical oscillators. These results are new phenomena that have not been revealed in typical electromagnetically induced transparent systems and may be applied to novel optical information-processing devices.

Methods In this letter, we begin with a dual-cavity magneto-optical mechanical system model. We analyze the composition of the cavity and provide the definition of each parameter. The magnon directly driven by the microwave source in the cavity a can directly establish a coupling mechanism with the microwave cavity photons. A YIG ball is placed in the maximum magnetic field of the microwave resonant cavity a . In order to bias the YIG ball, a uniform external bias magnetic field needs to be applied along the z direction. The cavity mode driving magnetic field in the y direction is mainly used to deform the YIG ball. The purpose of the dynamic magnetization of the magnon is to ensure that the cavity mode driving magnetic field in the y direction and the uniform external bias magnetic field along the z direction are perpendicular to the magnetic field of the cavity mode in the x direction at the same time. The Heisenberg equation of motion, factorization, and other methods are used to solve the obtained Hamiltonian, and the relational expression between the resonator field and the output field is established. Finally, we explore the different effects under different parameters. We investigate the coherent optical response under different parameter mechanisms, such as the coupling strength (J) between the resonators and the ratio (n) of the probing light intensity of the two resonators, in the case of system interaction, and the optical response transmission characteristics of the optomechanical system can be observed.

Results and Discussions This study shows that different properties can be observed in the cavity of a magnetomechanical system under different parameter mechanisms. In the case where the mechanical oscillator is coupled with the magnon and the probe light on the right is turned off ($n=0$), when the coupling strength $J < \kappa$, the greater the coupling strength J of the system, the more obvious the degree of transmission of the system. When the value of the coupling strength J increases to $J = \kappa$, the optomechanical system exhibits complete transmission at the central resonance, and when $J > \kappa$, the system exhibits mode splitting (Fig. 2). In the case where the microwave photons are coupled with the magnons and the probe light on the right is turned off ($n=0$), with an increase in the coupling strength J between the two resonators, the peak values of the transparent peaks on both sides gradually increase, while the central resonance strength gradually decreases. When the intensities of the left and right probe light are the same ($n=1$), the peak transmittance and reflectance of the left cavity increase with the increase of J . This is because of the quantum coherence between the left and right probe fields (Fig. 3). In the case where microwave photons, mechanical oscillators, and magnons are coupled together and the right probe light is turned off ($n=0$), when the coupling strength J between the two resonators is enhanced, the peak values of the transparent peaks on both sides gradually become larger, the peak value at the central resonance gradually becomes smaller, and the standard mode splitting phenomenon occurs. When the effective optomechanical coupling ratio is changed, the width of the transparent peak at the central resonance increases with an increase in the G value; the spacing between the transparent peaks on both sides also increases. Coupling with magnons also allows a portion of the energy to be stored in the magnons (Fig. 4). When the intensity of the probe light on the left and right sides of the system is the same ($n=1$), the transmission first increases and then decreases, and the reflection first decreases and then increases on both sides of the optical system. This phenomenon is very important

(Fig. 5). Based on this phenomenon, the dynamic control of the dynamic propagation process of weak light signals can be realized, which can be used to construct photonic devices with special functions.

Conclusions In this paper, based on an optomechanical system, a dual-resonator magneto-optomechanical system based on magnons is proposed. The numerical results achieved can be displayed analytically under the coupling of the magnon and mechanical oscillator, the coupling of the magnon and microwave photon, and the co-coupling of the three. The detection field is regulated by adjusting the system parameters. This dual-cavity magnetomechanical system can exhibit different optical transmission characteristics, such as mode splitting, perfect quantum expansion coherence, perfect quantum destructive coherence, and absorption of magnon energy, which are very important in the process of quantum information processing. Studying and manipulating these dynamic controls can help us understand phenomena related to cavity opto-mechanical systems from a new perspective. The proposed scheme may serve as a potential platform for realizing controllable photon transmission and developing novel photonic devices.

Key words quantum optics; magnon; cavity optomechanical system; coherent optical transmission